CrossMark

# Kinetics of *p*-Nitrophenol Reduction Catalyzed by PVP Stabilized Copper Nanoparticles

A. D. Verma[1] · R. K. Mandal[2] · I. Sinha[1]

Abstract Copper nanoparticles (CuNPs) in aqueous medium were prepared with alkaline hydrazine hydrate as the reductant and PVP as the stabilizing agent without any inert gas protection. Careful variation in the amount of reductant resulted in formation of two stable CuNPs dispersions with different average sizes and consequently different localized surface plasmon resonance absorbances. These two as-synthesized CuNPs dispersions were used to catalyze the model *p*-nitrophenol reduction reaction. The kinetics of reduction was monitored as a function of concentration and temperature of reactants. Using this we determined the activation energy, pre-exponential factor and the entropy of activation for the two types of CuNPs samples. Catalytic activities of the CuNPs were found to be affected mainly by their activation energies.

Graphical Abstract
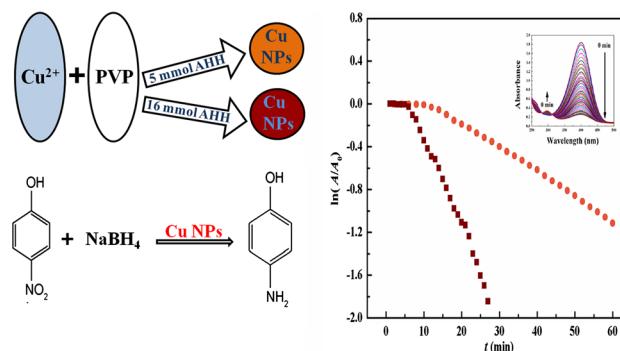
1 Introduction

The catalytic properties of metal nanoparticles differ significantly from their bulk counterparts and have been widely explored in recent years. The focus has been mainly on investigating the catalytic applications of nanoparticles of gold, platinum, palladium etc. [1–5]. In comparison to these, copper nanoparticles (CuNPs) as catalysts are much cheaper. They have also shown excellent catalytic activity in various reactions [6, 7]. Among the latter, the catalytic reduction of *p*-nitrophenol (NP) by NaBH₄ is especially important due to several reasons. One important reason is that this reaction fits the criteria for model reactions [8]. A model reaction is well controlled, does not have any side reactions, is relatively easy to analyse and requires mild conditions only. Kinetic analysis of such model reactions

✉ I. Sinha
isinha.apc@iitbhu.ac.in

1   Department of Chemistry, Indian Institute of Technology (Banaras Hindu University), Varanasi 221005, India

2   Department of Metallurgical Engineering, Indian Institute of Technology (Banaras Hindu University), Varanasi 221005, India

enable correlations between nanoparticle features and catalytic properties in a quantitative manner and thus provide insight into mechanistic aspects involved.

As a reaction, the reduction of NP has several advantages. First of all, this results in removal of NP which is an environmental pollutant [9]. Secondly, the product *p*-aminophenol (AP) is an important compound with several applications such as corrosion inhibitor, anticorrosion-lubricant, hair-dyeing agent etc. [10]. It is also an important intermediate in synthesis protocols of several drugs [11]. Reduction of NP can be carried out by either metal/acid reduction or by catalytic hydrogenation. Metal/acid reduction has disadvantages such as poor selectivity and corrosion due to use of acid. On the other hand, generally catalytic hydrogenation has been carried out in presence of costly noble metal catalysts. Therefore, the reduction of NP by $NaBH_4$ catalyzed by much cheaper CuNPs could be a more efficient route.

The chemical reduction route is a convenient method for the synthesis of copper nanoparticles. In this technique the nanoparticle characteristics can be controlled by varying the different experimental parameters like concentrations, redox potentials, temperature, and pH [12–14]. However, CuNPs under ambient conditions are susceptible to surface oxidation since Cu oxide phases are thermodynamically more stable than pure Cu [15]. Therefore, the synthesis of CuNPs has usually been attempted using strong reducing agents and inert atmosphere in non-aqueous media to prevent or minimize surface oxidation. The synthesis of CuNPs is also possible in alkaline pH conditions even in aqueous medium when hydrazine hydrate (HH) is used as the reductant. Such a synthesis does not require inert gas atmosphere due to in situ generation of N_2 [16–18]. The reductant was used in excess in these investigations. Here we use alkaline hydrazine hydrate (AHH) as reductant for aqueous phase preparation of CuNPs in presence of polyvinyl pyrrolidone (PVP) as the stabilizer. This enables better control of over different stages of CuNPs synthesis and varying the amount of AHH enables us to delineate different stages of growth of CuNPs.

The primary goal of this communication is to investigate the catalytic properties of these differently sized PVP stabilized pure CuNPs at different temperatures. There are few studies on reduction NP over CuNPs with little or no kinetic studies. Thus, recently Deka et al. [7] reported only the catalytic activity of in situ generated CuNPs (without using any stabilizer) for reduction of NP to AP at room temperature. Similarly, Prucek et al. [19] also reported polyacrylic acid (PAA) stabilized CuNPs catalyzed reduction of NP to AP. In both cases the presence of Cu_2O in CuNPs samples was noted by the authors. Recently, Kaur et al. [20] have also reported polyacrylic acid (PAA) stabilized CuNPs (without any Cu_2O formation) catalyzed reduction of NP to AP.

2 Experimental Details

2.1 Synthesis of CuNPs Stabilized by PVP

Materials used for the synthesis of copper nanoparticles were $Cu(NO_3)_2 \cdot 3H_2O$ (Merck), polyvinylpyrrolidone (PVP) (Himedia), NaOH (Merck), and HH (Merck). All reagents used were of analytical reagent grade and used without further purification. Equal volumes of 0.0025 M NaOH and 0.05 M HH were mixed to prepare the AHH solution (with pH 9). The copper salt solution was prepared by adding 10 wt% PVP to 5 mL aqueous solution of 0.01 M $Cu(NO_3)_2 \cdot 3H_2O$. The AHH solution was now added in a drop wise manner to the copper salt solution with continuous stirring. The final reaction is $2Cu^{2+} + N_2H_4 + 4OH^- \rightarrow 2Cu + N_2 + 4H_2O$ [16, 21]. As the amount of AHH added was increased the initially blue colored copper salt solution changed first to yellow, then orange, and finally to a reddish-brown color with precipitate formation. Now two different samples S1 and S2 corresponding to stable orange and reddish brown stages were prepared. For these, 5 and 16 mmol AHH were added to separate precursor solutions ($Cu(NO_3)_2 \cdot 3H_2O$ with 10 wt% PVP) for preparation of samples S1 and S2. The reaction vessel was closed immediately after AHH addition. Figure 1 shows the as prepared S1 (orange) and S2 (reddish-brown) CuNPs sol samples. In general, the prepared samples were found to be stable for at least 4 weeks in closed conditions.
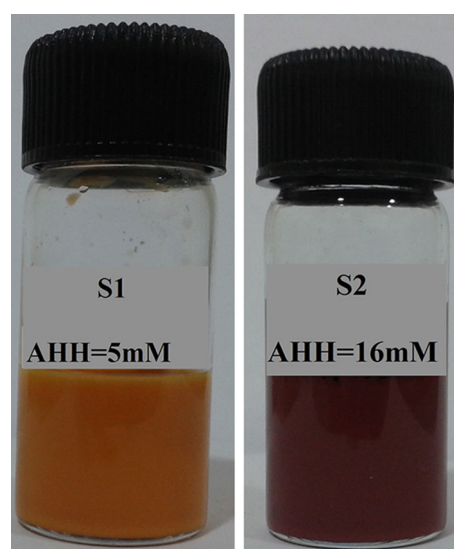

Fig. 1 Freshly prepared *orange* (*S1*) and *reddish-brown* (*S2*) CuNPs sols

2.2 Reduction of *p*-Nitrophenol

The as prepared CuNPs samples S1 and S2 were diluted by thirty times before using them as catalyst for NP reduction. After dilution the concentrations of sample S1 and S2 were 0.0019 and 0.0017 mg/mL respectively. 0.1 mL of 1.2×10^{-3} M NP was diluted by adding 1.85 mL water and taken in a standard quartz cuvette of 1-cm path length. To this 50 μL of aqueous 0.1 M $NaBH_4$ solution was added. Then 100 μL of the diluted CuNPs sol sample was added. Typically the pH of the reaction mixture was found to be around 9.5. The absorption spectrum was recorded after every 2 min time interval. The same procedure was repeated to monitor the kinetics of CuNPs catalyzed reaction at four temperatures 292, 296, 300 and 304 K. The effect of variation of reactant concentration on the kinetics was also measured. All reactions done for this purpose were conducted at 300 K. For studying the effect of increasing $NaBH_4$ concentration 0.1 mL of 1.2×10^{-3} M NP was diluted by adding 1.85 mL water. To this 50 μL of aqueous $NaBH_4$ solution of different concentrations (0.1, 0.2, 0.3, 0.4 M) were added. Then 100 μL of the diluted CuNPs sol sample was added and the absorption spectrum was recorded after every 2 min time interval for each concentration of $NaBH_4$. Similarly, the effect of increasing NP concentration on the kinetics of the reaction was also investigated. Here the concentration of $NaBH_4$ was fixed at 0.1 M while NP concentrations used were 0.3, 0.6, 1.2, 1.8×10^{-3} M.

2.3 Analysis

The UV–Vis absorption spectra of the CuNPs aqueous dispersions were recorded on a Perkin Elmer XLS spectrophotometer and Agilent Cary 60 spectrophotometer. The TEM studies of the CuNPs samples were carried out with FEI Technai-20 G^2 operating at voltage of 200 kV. FT-IR spectra were recorded with a Fourier-transform infrared spectrophotometer (Nicolet 6700) between 4000 and 400 cm^{-1}, with a resolution of 0.09 cm^{-1}.

3 Results and Discussion

3.1 Characterization of CuNPs Stabilized by PVP

To understand interactions between CuNPs and the polymeric stabilizer, the FT-IR spectra of PVP and CuNPs stabilized by PVP were compared (Fig. 2). The peak at 1660 cm^{-1} (PVP FTIR) corresponds to the C=O vibrational mode. On the contrary, the FT-IR spectrum of PVP stabilized CuNPs displayed a weak red-shifted C=O peak at 1640 cm^{-1} [22]. A sharp band at 1290 cm^{-1} shown by

PVP FT-IR was found to be weakened in Cu–PVP spectrum, indicating the change in dipole moment of C–N bond. Furthermore, the peak at 650 cm^{-1} in PVP disappeared in the Cu–PVP spectrum due to the Cu ion interaction with C–N bond. It appears PVP chemisorbs on to the CuNPs surface using its carbonyl oxygen and the ring nitrogen affecting the surface electron density and thereby the localized surface plasmon resonance (LSPR) properties of these nanoparticles.

The TEM micrographs of the prepared CuNPs samples and the corresponding electron diffraction patterns are shown in Fig. 3. The average size of CuNPs in sample S1 is found to be ~11 nm from its TEM images (Fig. 3a). Here the nanoparticles appear to be embedded in some kind of PVP polymer matrix. On addition of more AHH, the CuNPs (sample S2) average size further decreases to ~9 nm (Fig. 3c). Figure 3b, d display the electron diffraction patterns of CuNPs samples S1 and S2 respectively. Indices of first four rings are indicated in Fig. 3b, d. The ring patterns of the samples could be indexed to FCC copper. This eliminates the possibility of oxidation of Cu nanoparticles.

Figure 4 shows the LSPR absorbance behaviour of the prepared CuNPs aqueous dispersions. Sample S1 displays a broadened featureless absorbance at about 500 nm indicating the presence of very small separated Cu nanoparticles embedded in the polymer matrix. The LSPR absorbance spectrum of the sample S2 on the other hand shows a prominent maximum at 593 nm which compares well with the characteristic plasmon absorption band of CuNPs. The shift in LSPR from 500 to 593 nm from S1 and S2 samples is presumably due to change in medium in
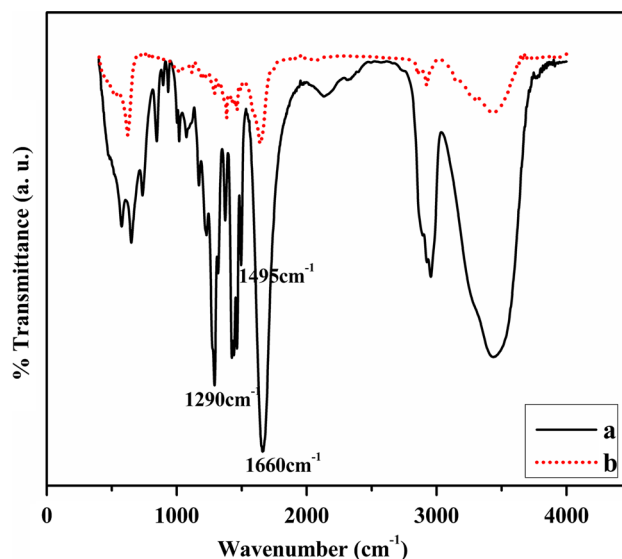

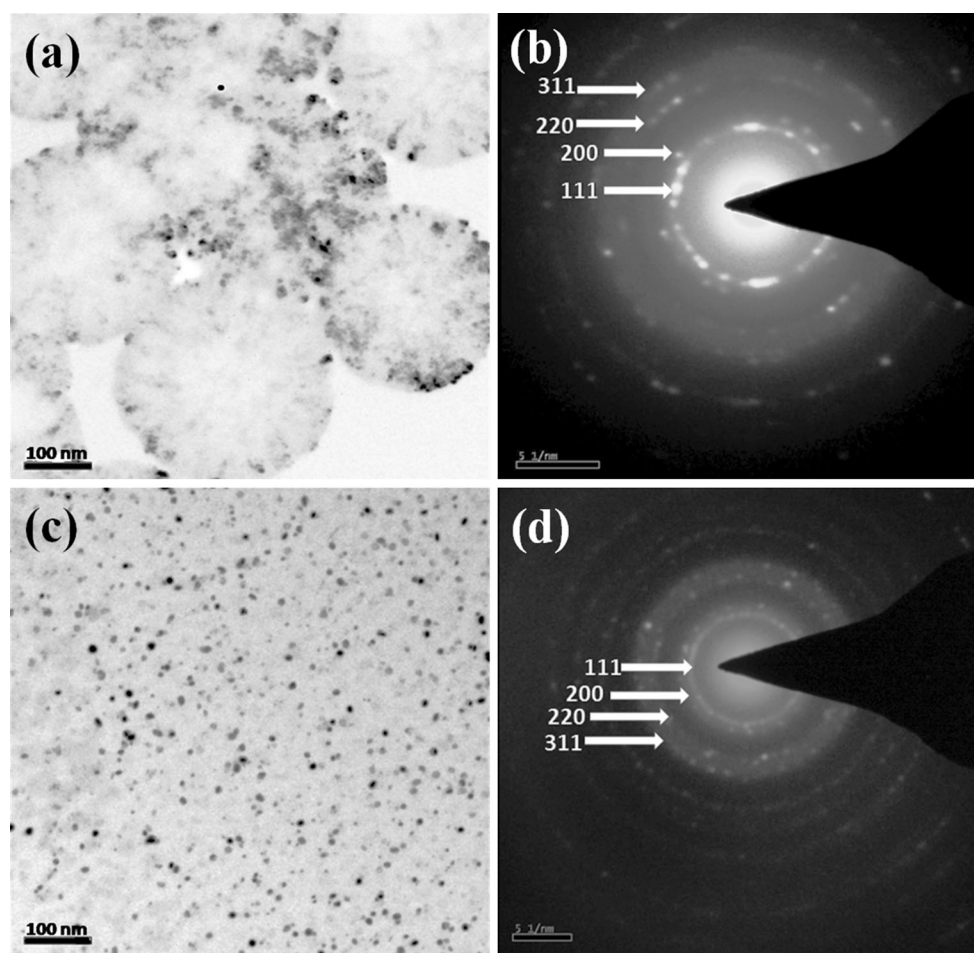**Fig. 2** FT-IR spectra of pure PVP (*a*) and CuNPs stabilized by PVP (*b*)

Fig. 3 TEM images of the two CuNPs sols samples: S1 (**a**), S2 (**c**), and their corresponding electron diffraction patterns: S1 (**b**), S2 (**d**), respectively
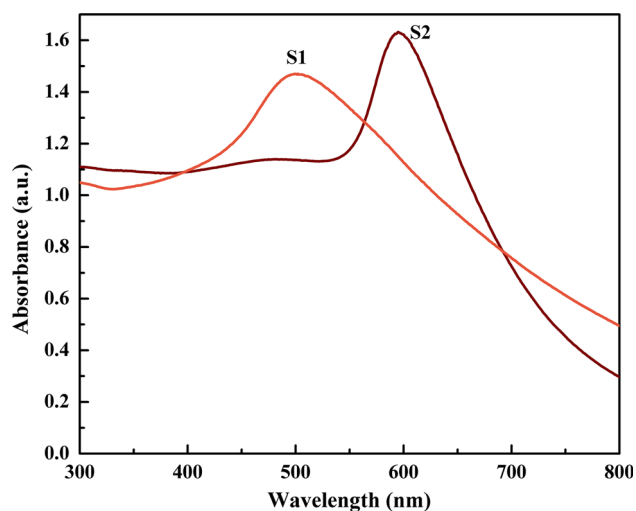

Fig. 4 The UV–Vis absorption spectra of CuNPs with different amounts of AHH: 5 mmol for S1, and 16 mmol for S2

which the CuNPs are dispersed. For the preparation of both CuNPs samples the amount of AHH added was in excess of the stoichiometrically required amount. That is, amount of excess AHH used to obtain S1 CuNPs is significantly different from that added to prepare S2 CuNPs. Hence, after synthesis, as compared to the S2 aqueous dispersion, less of undecomposed (or excess) HH is present in S1 dispersion. We believe that different amounts of excess AHH changes the dielectric environment and this may be the reason for the LSPR change observed.

The two stable stages (orange and reddish brown) were obtained in the same sol preparation with gradual increase in amount of AHH added. Therefore, the nanoparticles formed at the initial (yellow) stage were also there in the penultimate (reddish brown) stage and we may conclude that the average particle size became finer with increase in AHH addition. This could be explained by two possible mechanisms which may both be happening. One possibility

is that the initial CuNPs formed at the first stage were some kind of aggregates of finer particles which broke into constituent particles on further addition of AHH. This may be due to heterogeneous nucleation density concentrated in a region with limited volume available for growth. The other alternative is that the nucleation rate increased with AHH addition (promoting homogeneous nucleation) resulting in finer nanoparticle sizes. To the best of our knowledge such separation of CuNPs growth stages has not been reported in earlier investigations following HH reductant addition to alkaline copper salt solution protocol.

3.2 CuNPs Catalyzed NP Reduction

The results of the reduction of NP to AP catalyzed by CuNPs with an excess amount of $NaBH_4$ are presented in Fig. 5a. The neutral NP solution exhibited a strong absorption peak at 317 nm. On addition of $NaBH_4$, due to the formation of *p*-nitrophenolate ion, the maximum absorbance shifted to 401 nm. Figure 5a shows that as the reduction of NP progressed with time the absorption peak at 401 nm decreased in intensity. Simultaneously, a smaller absorbance maximum at 300 nm gradually increased due to formation of the reaction product AP. Also, the spectrum shows two isosbestic points at 281 and 311 nm which indicate that NP was fully converted to AP without any side reaction [20]. Figure 5b shows the UV–Vis of the blank sample, that is, without CuNPs catalyst. It was observed that there was no change in the maximum absorbance of *p*-nitrophenolate ion at 401 nm even after 70 min confirming that no reduction occurs in absence of catalyst.

Let A and A_0 denote the absorbance of *p*-nitrophenolate ions at time t and t_0, respectively. Then a plot of $\ln(A/A_0)$

against time (Fig. 6) showed that initially there was a time gap (the induction time t_{ind}) during which no reduction took place. Thereafter, a linear plot was obtained (Fig. 6) from which we inferred pseudo first-order kinetics since the concentration of $NaBH_4$ (taken in excess relative to NP) was virtually constant throughout the reaction. These observations are in agreement with previous literature data on metal-catalyzed reduction of NP [7, 23]. The apparent rate constant (k_{app}) was determined in a straightforward manner from the slope of the linear fit of $\ln(A/A_0)$ with time t (after excluding t_{ind}). It can also be observed in Fig. 6, that the k_{app} of the reduction catalyzed by S1 CuNPs is lesser than the k_{app} obtained using S2 ones.

The effect of reactant concentration is displayed in Fig. 7a, b, in which k_{app} is plotted as a function of concentration of sodium borohydride and NP, respectively at a constant temperature. It was found, that the k_{app} increased almost in a linear fashion with the concentration of $NaBH_4$. On the other hand, k_{app} showed rapid (almost exponential) decrease with increase in the NP concentration. This can explained if we assume that as in reference [24] the catalytic reduction proceeds on the surface of the metal nanoparticles by the Langmuir–Hinshelwood (LH) mechanism and the adsorption constant of NP onto CuNPs catalyst surface is much higher than that of $NaBH_4$. In reference [24] the authors found that adsorption constant of NP is about 100 times that of $NaBH_4$ on to the catalyst surface. A high concentration of NP molecules led to nearly full coverage of the surface of the nanoparticles by NP [24]. In the LH mechanism borohydride ions and NP molecules adsorb on to the surface of the nanoparticles and the rate-determining step is the reduction of NP by the adjacently located surface-hydrogen species [8]. Finally, the product AP formed is desorbed as soon as it is formed
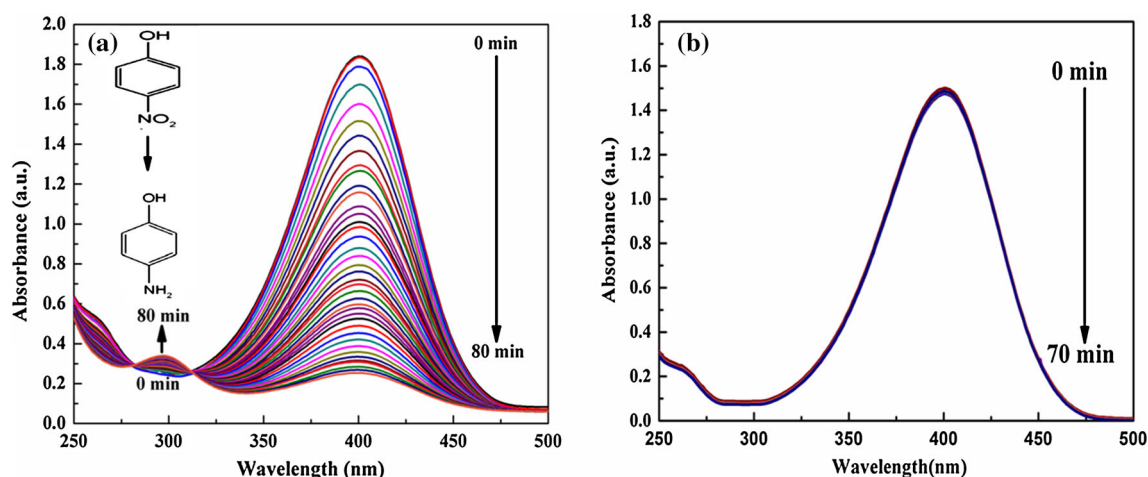

Fig. 5 The UV–VIS absorption spectra of *p*-nitrophenol versus time (with CuNPs catalyst) (**a**) and for the blank sample (without CuNPs catalyst) (**b**)
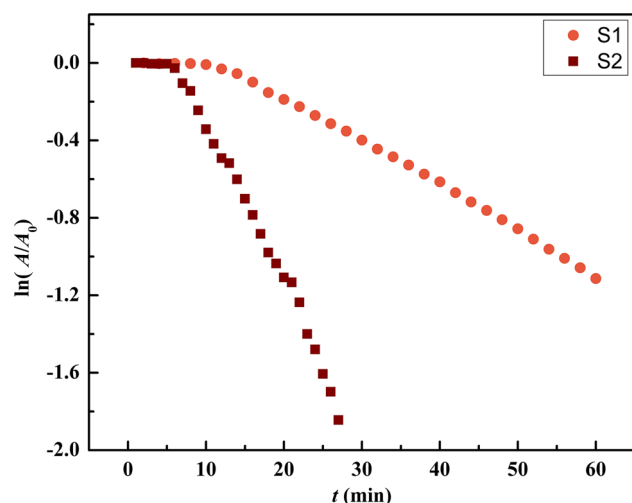
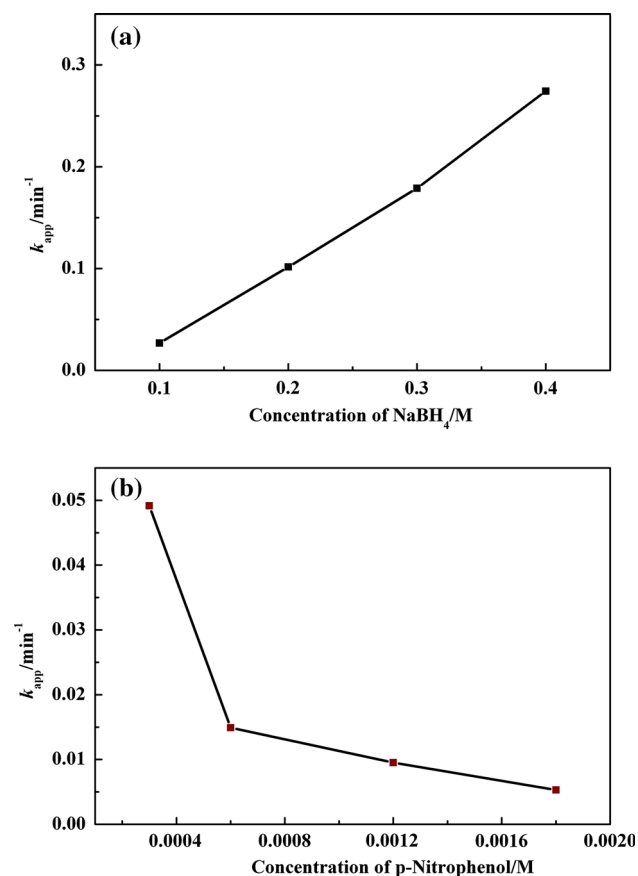**Fig. 6** Variation of ln A/A_0 [absorbance (A) was measured at $\lambda = 401$ nm] versus time

Fig. 7 Variation of k_{app} as a function of different initial concentrations of reactants with NaBH$_4$ (0.1, 0.2, 0.3, 0.4 M) at c(NP) $= 1.2 \times 10^{-3}$ M and m(CuNPs) $= 0.0036$ mg constant (**a**); and that of NP (0.3, 0.6, 1.2, 1.8 $\times 10^{-3}$ M), at c(NaBH$_4$) $= 0.1$ M, m(CuNPs) $= 0.0036$ mg (**b**)

and therefore does affect the kinetics. Combining the information pertaining to respective adsorption constants of the reactants with LH mechanism implies that in present system competition between reactants for active sites on the catalyst surface slows down the reaction. An optimum concentration of NP and NaBH$_4$ is therefore required for the achieving the maximum reaction rate.

To facilitate effective comparison of k_{app} of different nanocatalysts available in literature we also calculated the k_{app} per mg of the nanocatalyst. The data, comparing various some typical CuNPs studies in this area, are given in Table 1. From Table 1, one can see that the rate constant obtained for both the CuNPs samples of this study are significantly higher compared to other values in literature [7, 20]. We also observe that the k_{app} per mg of the nanocatalyst S2 is significantly higher (about six times) than that obtained when catalyzed by S1 CuNPs. This could be due to either the following factors or a combination of both.

One of the factors affecting the catalytic activity could be the size difference between the two CuNPs synthesized in the present study. Finer particle size would mean higher surface area or more number of surface active catalytic sites. However, the size difference between S1 and S2 CuNPs is relatively small, which cannot justify such a large difference in catalytic activity. Alternatively, higher catalytic activity of S2 (compared to S1) could be because of associated inherently different activation energies. Accordingly, to find the activation energies associated with S1 and S2 catalysts the NP reduction was carried out at different temperatures. These experiments showed that k_{app} for a given CuNPs nanocatalyst increased with temperature and could be analysed in terms of the classical Arrhenius equation. Figure 8 shows ln k_{app} versus $1/T$ plots for nanocatalyst samples S1 and S2. Good linear fits were obtained in case of both plots as per the linearized Arrhenius Eq. (1).

$$\ln k_{app} = \ln A - E_a/RT \tag{1}$$

The activation energy (E_a) was obtained from the slope ($-E_a/R$) of the linear fits to the plots. The activation energy of sample S2 (Table 2) was found to be nearly half of the value obtained for S1 nanoparticles. Therefore, it appears that the much higher catalytic activity obtained for S2 CuNPs was predominantly owing to its significantly lower activation energy. In addition to activation energy, Table 2 also gives the pre-exponential factor (A) calculated from the intercept of the linear dependence of ln k versus $1/T$, and the entropy of activation (ΔS) obtained from the relation ln $A = \Delta S/R$ [25]. As the activation energy increases, the pre-exponential factor and consequently the entropy of

Table 1 Comparison of different reported apparent reaction rates k_{app} for CuNPs catalyzed *p*-nitrophenol reduction

Composition	Apparent reaction rate (min^{-1})	Apparent reaction rate (per mg of CuNPs) (min^{-1})	Reference
Cu–PVP (S1)	4.92×10^{-2}	12.29	This work
Cu–PVP (S2)	2.63×10^{-1}	73.08	-do-
Cu	9.55×10^{-2}	7.64×10^{-3}	[2]
Cu–PAA	5.94×10^{-2}	3.88	[23]
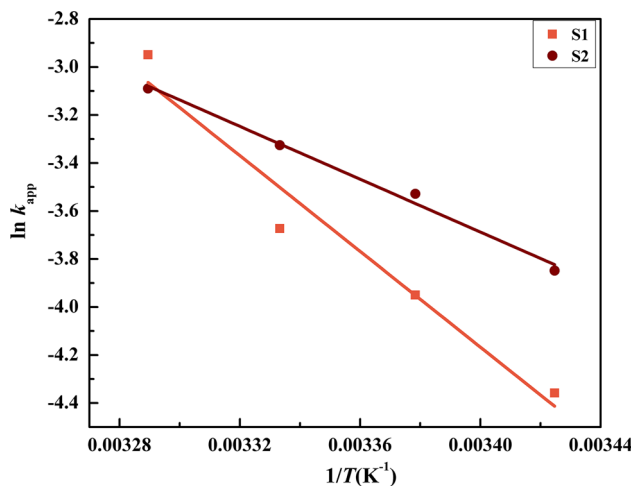
Fig. 8 Arrhenius plots for reactions catalyzed by S1 and S2 CuNPs, respectively

Table 2 Activation energy (E_a), pre-exponential factors (A), and the entropy of activation (ΔS) for S1 and S2 Cu NPs

Cu NPs	Size (nm)	Activation energy (E_a) (kJ/mol)	Pre exponential factor (A) (min^{-1})	Entropy of activation (ΔS) (J/mol K)
S1	~ 11	82.96	8.4×10^{12}	247.2
S2	~ 9	45.76	3.3×10^{6}	124.9

activation also increases. The activation energy, pre-exponential factor and the entropy of activation values found for S2 CuNPs compare favourably with the values given in references [1, 26]. It is also noteworthy that this is first report in the area of Cu nanoparticle catalyzed NP reduction reactions which has investigated the activation energy, the pre exponential factor and the entropy of activation.

4 Conclusions

The controlled addition of AHH (reductant) in presence of PVP to the copper salt solution resulted in two stable aqueous sols of CuNPs with different average sizes (9 and

11 nm) and LSPR absorbance values. This may be due to lesser nucleation rate for smaller AHH addition and further increase in nucleation rate on excess AHH addition. These CuNPs were then utilized as catalysts for reduction of NP to AP. In accordance with the Langmuir–Hinshelwood mechanism, the rate constant increased with the concentration of the reductant and decreased in almost an exponential fashion with increase in NP concentration. The catalytic activities of the PVP stabilized CuNPs catalysts prepared in the present study were found to be significantly higher than other CuNPs reported earlier in literature. The much lower activation energy found for the smaller CuNPs as compared to the other CuNPs catalyzed NP reduction appears to be the predominant reason for it.

References

1. Zeng J, Zhang Q, Chen J, Xia Y (2010) Nano Lett 10:30
2. Gao Z, Su R, Huang R, Qi W, He Z (2014) Nanoscale Res Lett 9:404
3. Johnson JA, Makis JJ, Marvin KA, Rodenbusch SE, Stevenson KJ (2013) J Phys Chem C 117:22644
4. Mei Y, Lu Y, Polzer F, Ballauff M (2007) Chem Mater 19:1062
5. Pandey S, Mishra SB (2014) Carbohydr Polym 113:525
6. Karakhanova EA, Maximova AL, Kardashevaa YS, Skorkin VA, Kardasheva SV, Predeinaa VV, Talanovaa MY, Lurie-Lukeb E, Seeleyb JA, Cronb SL (2010) Appl Catal A 385:62
7. Deka P, Deka RC, Bharali P (2014) New J Chem 38:1789
8. Herves P, Perez-Lorenzo M, Liz-Marzan LM, Dzubiella J, Lu Y, Ballauff M (2012) Chem Soc Rev 41:5577
9. Dieckmann MS, Gray KA (1996) Water Res 30:1169
10. Zaharia I, Diaconu I, Ruse E, Nechifor G (2012) Dig J Nanomater Bios 7(3):1303
11. Patil D, Nag S, Basak A, Nag A (2008) Int J Chem Sci 6(1):11
12. Goia DV (2004) J Mater Chem 14:451
13. Sergeev GB (2001) Russ Chem Rev 70:809
14. Singh M, Sinha I, Mandal RK (2009) Mater Lett 63:425
15. Chang SJ, Tung CA, Chen BW, Chou YC, Li CC (2013) RSC Adv 3:24005
16. Wu SH, Chen DH (2004) J Colloid Interface Sci 273:165
17. Deng D, Jin Y, Cheng Y, Qi T, Xiao F (2013) ACS Appl Mater Interfaces 5:3839
18. Singh M, Sinha I, Premkumar M, Singh AK, Mandal RK (2010) Colloids Surf A 359:88
19. Prucek R, Kvitek L, Panacek A, Vancurova L, Soukupova J, Jancik D, Zboril R (2009) J Mater Chem 19:8463
20. Kaur R, Giordano C, Gradzielski M, Mehta SK (2014) Chem Asian J 9:189
21. Grouchko M, Kamyshny A, Ben-Ami K, Magdassi SJ (2009) Nanopart Res 11:713

22. Xian J, Hua Q, Jiang Z, Ma Y, Huang W (2012) Langmuir 28:6736
23. Yang X, Zhong H, Zhu Y, Jiang H, Shen J, Huang J, Li C (2014) J Mater Chem A 2:9040
24. Wunder S, Polzer F, Lu Y, Mei Y, Ballauff M (2010) J Phys Chem C 114:8814
25. Narayanan R, E-Sayed MA (2004) Nano Lett 4:1343
26. Noh JH, Meijboom R (2014) Appl Surf Sci 320:400